Vibrations and Thermodynamics of Clusters of Polycyclic Aromatic Hydrocarbon Molecules: The Role of Internal Modes

Mathias Rapacioli

Institut für Physikalische Chemie und Elektrochemie, TU Dresden, Mommenstrassse 13, D-01062 Dresden, Germany

Florent Calvo*

Laboratoire de Chimie et Physique Quantiques, IRSAMC, Université Paul Sabatier Toulouse 3, 118 Route de Narbonne, 31062 Toulouse Cedex, France

Christine Joblin

Centre d'Étude Spatiale des Rayonnements, CNRS-Université Paul Sabatier Toulouse 3, Observatoire Midi-Pyrénées, 9 Av. du colonel Roche, BP 4346, 31028 Toulouse Cedex 4, France

Pascal Parneix

Laboratoire de Photophysique Moléculaire, CNRS Bât 210, Université Paris-Sud, 91405 Orsay Cedex, France

Fernand Spiegelman

Laboratoire de Chimie et Physique Quantiques, IRSAMC, Université Paul Sabatier Toulouse 3, 118 Route de Narbonne, 31062 Toulouse Cedex, France

Received: December 21, 2006; In Final Form: February 12, 2007

The vibrational spectra of clusters of coronene molecules are theoretically calculated using a mixed quantum/classical scheme, each molecule being described by a tight-binding Hamiltonian, the intermolecular forces being provided by explicit Lennard-Jones and point charge sites. The normal modes of vibrations are shown to exhibit significant variations upon clustering. In particular, for large clusters intra- and intermolecular modes tend to mix and fill the mid-infrared range. We also calculate the heat capacity of the $(C_{24}H_{12})_8$ cluster as a function of temperature, emphasizing the isomerizations that take place during melting. Quantum delocalization effects, as obtained from the Pitzer−Gwinn semiclassical approximation, are important enough to wash out all signatures of the structural transitions on the caloric curve. On the basis of a simple two-state model we estimate that clusters containing about 300 molecules are required for melting to be detected on the caloric curve.

I. Introduction

Infrared spectroscopy has become a powerful way of identifying the structure and even the dynamics of complex organic molecules in gas or solvated phases. The advances brought by IR spectroscopy have been quite spectacular for peptides,[1−3] aromatic molecules,[4,5] or hydrogen-bonded complexes,[6,7] in particular, water, methanol, or ammonia clusters.[8−10] IR spectroscopy is also a standard tool in astronomical observations. The aromatic infrared bands measured in many regions of the interstellar medium were interpreted by Léger et al.[11] and by Allamandola et al.[12] as the likely signature of polycyclic aromatic hydrocarbons (PAHs). As suggested by the brightness of these features, PAHs could represent up to 20% of all carbon in the Universe, putting them among the most abundant complex organic molecules.[13] As a result, they should play an important role in the energetic budget and chemistry of the Galaxy.

Many laboratory studies,[14−24] including neutron scattering measurements,[25,26] as well as force field[27,28] and quantum chemistry calculations,[29−39] on single PAH molecules have been performed in the past, but no identification of individual molecules in space could be achieved yet. From the astronomical side, the observations of the European Infrared Space Observatory led Cesarsky et al.[40] to reveal the presence of very small carbon grains, which were suggested by Rapacioli et al.[41] to be clusters of PAH molecules. Other observations from the Spitzer Space Telescope analyzed by Berné et al.[42] confirmed this result. The forthcoming Herschel Space Observatory should be able to search for bands associated with the very low-frequency modes of free flying PAHs and PAH clusters in the far-IR range.[43,44]

Beyond astrochemistry, the study of PAH clusters is also of great interest in the field of combustion.[45,46] Polycyclic aromatic hydrocarbon molecules could be involved as a step leading to soot formation, a still-standing problem where PAHs are believed to mark the transition between different growth mechanisms.[45−47]

While significant work has been devoted to isolated PAHs, clusters of PAH molecules are much less documented. Experimental[48−51] and theoretical[50,52−57] investigations have generally focused on small aggregates of usually small PAHs

10.1021/jp068821z CCC: $37.00
Published on Web 03/30/2007

(typically, naphthalene or anthracene), far below the 400 carbon atoms astrophysical limit.[42] Clusters of coronene ($C_{24}H_{12}$) molecules containing up to 20 units have been produced in a gas aggregation source by Schmidt and co-workers.[58,59] These authors showed that the dissociation of coronene clusters induced by multiphoton excitation of a near-UV laser proceeds via the ejection of van der Waals-bonded coronene units.

We previously[60] investigated the stable structures of polycyclic aromatic hydrocarbon clusters containing up to 800 carbon atoms, for PAH molecules ranging from pyrene ($C_{16}H_{10}$) to circumcoronene ($C_{54}H_{18}$). In agreement with other studies on small agreggates,[50,54,55,57] the most stable structures were found to be made of stacks. At small sizes, a single stack is formed. After a critical size is reached, depending on the PAH itself, the lowest energy structures consist of multiple stacks lying next to each other.[60] The atomistic model used in that work was recently used in molecular dynamics simulations to study the nucleation and decay mechanisms in PAH clusters.[61]

In the present paper, we address more specifically the issues of vibrational and thermodynamical properties of PAH clusters, aiming at characterizing the specific effects of aggregation. Seahra and Duley[62] investigated the vibrations in PAH clusters, in the approximation of one-dimensional stacks. These authors showed that the cluster modes lie in the approximate frequency range between 25 and 120 wavenumbers. In the context of astronomical observations, it is of fundamental interest to extend these studies to the mid- and near-infrared ranges, where intramolecular PAH modes are expected to be important. The purely intermolecular potential used in ref 60 lacks a proper description of these internal modes, hence we have complemented our explicit potential with a suitable, quantum tight-binding model initially developed for isolated PAH molecules.[63]

We also wish to characterize the caloric curve of a typical PAH cluster, namely the coronene octamer, from this combined model. As shown by Schmidt et al.[59] the thermal excitations of inner- and intermolecular modes are very different in magnitude, and the contribution of internal modes is clearly dominant on the caloric curve, essentially because the latter are more numerous. In particular, strong quantum vibrational effects at low temperature should be expected, associated with the inner degrees of freedom. On the basis of mass spectroscopic measurements interpreted in the framework of the evaporative ensemble,[64] Schmidt and co-workers[59] estimated that coronene clusters were stable up to about 470 K on the 500 μs time scale, while the single coronene molecule starts to dissociate via hydrogen emission above 2000 K within 10 μs. The thermodynamical properties of the isolated coronene molecule have been calculated and discussed previously.[43,44,65] Sallamie and Shaw[38] combined experimental and theoretical data to calculate the constant pressure C_P and constant volume C_V heat capacities of bulk coronene in the solid state, assuming Debye expressions for C_V and empirical equations of states to estimate the $C_P - C_V$ differences. It should be stressed here that the measured C_P data due to Wong and co-workers[66] exhibit an extended anomaly in the range 215−250 K, which was attributed by the authors to several experimental difficulties. More recent data obtained by Chickos et al.[67,68] do not show this anomaly. Here we have calculated the heat capacity of a PAH cluster by performing classical Monte Carlo simulations, and correcting for quantum vibrational effects using the Pitzer−Gwinn[69] approximation.

The article is organized as follows. In the next section, we describe the atomistic models used for clusters of PAH molecules, including the explicit intermolecular potential and the intramolecular tight-binding contributions. In section III, we briefly describe the calculation of vibrational frequencies, and how the contributions of the intermolecular and internal modes were separated. In this section we also present and discuss our results on the vibrational spectra for coronene clusters containing up to 8 molecules. In section IV, the methods for calculating the heat capacity are presented and the caloric curves are discussed in the light of the isomerization processes that take place at various temperatures. We finally summarize and conclude in section V.

II. Model

Following our previous work on structural properties,[60] clusters of neutral PAH molecules are modeled using simple pairwise site−site Lennard-Jones and point charges forces, assuming that the molecules remained frozen at the equilibrium geometry of the monomer. The potential energy $V_{\text{inter}}(i,j)$ between molecules i and j reads

$$V_{\text{inter}}(i,j) = \sum_{\alpha \in i} \sum_{\beta \in j} [V_{\text{LJ}}(r_{i\alpha\, j\beta}) + V_Q(r_{i\alpha\, j\beta})] \qquad (1)$$

where $V_{\text{LJ}}(r_{i\alpha\, j\beta})$ is the dispersion−repulsion energy between atoms i_α of molecule i and j_β of molecule j, and V_Q denotes the electrostatic interaction between the partial charges carried by the atoms. The Lennard-Jones parameters used for the dispersion−repulsion energy are taken from van de Waal,[52] and the partial charges were fitted from DFT/B3LYP electronic structure calculations to reproduce the electrostatic potential around the gas-phase coronene molecule.[60] More details about the molecular geometry and the partial charges used in the present work are given in ref 60.

In order to include intramolecular interactions at a reasonable computational level, we use a simple quantum tight-binding (TB) scheme to model the intramolecular interactions. For a cluster containing N_{mol} molecules, the total Hamiltonian of the system is thus written

$$H_{\text{total}} = \sum_{i=1}^{N_{\text{mol}}} H_{\text{intra}}(i) + \sum_{i<j} V_{\text{inter}}(i,j) \qquad (2)$$

the TB Hamiltonian of molecule i being here denoted as $H_{\text{intra}}(i)$. We use for H_{intra} the tight-binding model developed by Nguyen-Thi et al.[63] This model was fitted to reproduce energetic and vibrational properties of isolated PAH molecules.[63] We did not change its original parameters. In Table 1 we have listed the set of harmonic frequencies of the isolated coronene molecule obtained with the present TB model, as well as corresponding data from previous recent investigations by other authors. Fleischer and Pulay[27] fitted a semiempirical force field to reproduce DFT/B3LYP calculations on benzene, and transferred this force field to the study of coronene vibrations. The increasing computational power allowed Sallamie and Shaw[38] to perform directly similar density functional calculations on $C_{24}H_{12}$.

As can be seen from Table 1, the present TB model compares very well with more sophisticated calculations, all vibrational frequencies falling within 2% at most from these benchmark values. Considering that DFT frequencies should be scaled by a factor in the range 0.96−0.98 (see, e.g., ref 31) in order to reach experimental agreement, the present values are indeed very satisfactory. The vibrational spectra also agree with inelastic neutron scattering data[25,26] and with Raman spectroscopy measurements on solid-state coronene.[70]

TABLE 1: Vibrational Frequencies for Gas-Phase Coronene

method	source	wavenumbers (cm^{-1})										
DFT	ref 38	90.6	90.8	130.5	167.5	232.2	303.0	303.3	307.3	307.6	376.2	376.3
B3LYP		390.2	390.7	463.9	465.1	483.7	492.0	507.0	507.2	526.1	537.8	559.1
6-31G		560.2	567.0	572.2	654.9	672.3	672.8	690.1	701.3	701.4	711.9	745.1
		745.6	790.1	799.7	800.0	823.5	825.3	826.5	826.6	871.8	871.9	896.1
		946.8	983.0	991.4	991.8	1004.9	1005.9	1013.1	1017.0	1017.0	1054.5	1176.1
		1176.8	1186.3	1196.3	1202.2	1202.4	1217.3	1252.6	1252.7	1261.3	1262.3	1262.4
		1282.4	1352.3	1352.3	1379.9	1384.3	1432.7	1433.0	1435.0	1435.1	1469.5	1470.1
		1470.2	1492.2	1493.6	1524.8	1543.6	1543.9	1581.6	1583.6	1639.1	1654.7	1654.8
		1655.6	1655.9	3155.8	3156.5	3157.1	3158.6	3158.8	3159.6	3177.0	3178.0	3178.6
		3180.3	3180.6	3182.2								
force field	ref 27	87.7	87.7	127.6	163.3	223.8	295.8	295.8	297.8	297.8	367.0	367.0
		380.2	380.2	446.7	446.7	468.3	478.2	494.8	494.8	515.7	544.6	544.6
		555.6	558.6	623.9	643.8	658.5	658.5	670.7	680.8	680.8	758.4	758.4
		759.6	778.0	778.0	780.1	800.8	800.8	803.1	803.1	837.1	837.1	857.3
		926.6	932.6	934.0	934.0	945.0	945.0	952.6	989.6	989.6	1029.0	1134.2
		1134.9	1134.9	1154.8	1154.8	1167.0	1178.5	1205.7	1205.7	1211.0	1216.9	1216.9
		1229.9	1318.2	1318.2	1334.5	1340.2	1388.7	1388.7	1393.7	1393.7	1417.9	1433.8
		1433.8	1446.5	1446.5	1484.1	1500.8	1500.8	1538.0	1550.9	1603.4	1615.4	1615.4
		1619.2	1619.2	3038.4	3039.4	3039.4	3041.3	3041.3	3042.4	3055.4	3056.7	3056.7
		3058.9	3058.9	3060.5								
TB	this work	92.2	92.2	130.5	163.5	242.6	308.0	308.0	310.6	310.6	378.3	378.3
		408.9	408.9	476.7	476.7	499.4	524.6	524.6	565.6	576.1	585.6	585.6
		589.4	595.1	693.6	713.8	728.2	728.2	731.1	746.9	746.9	832.4	838.5
		838.5	849.6	849.6	908.2	908.2	926.9	926.9	937.8	937.8	955.4	961.3
		1017.2	1106.3	1109.6	1109.6	1118.1	1122.4	1122.4	1130.4	1130.4	1134.6	1189.1
		1229.8	1229.8	1277.3	1277.3	1297.8	1300.8	1313.7	1313.7	1316.2	1316.2	1323.2
		1382.8	1402.6	1407.6	1407.6	1409.2	1431.2	1431.2	1470.4	1470.4	1489.4	1524.6
		1524.6	1569.3	1596.4	1596.4	1635.8	1641.8	1641.8	1653.3	1653.3	1669.2	1671.9
		1671.9	1693.4	3115.8	3116.0	3116.0	3116.5	3116.5	3116.8	3124.6	3124.9	3124.9
		3125.5	3125.5	3125.7								

The TB model was incorporated into the intermolecular energy surface in a parallel fashion using the OpenMP protocol. However, even with a nearly linear scaling with the number of molecules, diagonalizing the quantum Hamiltonian a statistically relevant number of times takes a significant computer time. In comparison, the intermolecular potential V_{inter} is computationally cheap, and allows an efficient sampling of the potential energy surface by Monte Carlo methods (note, however, that the global optimization of PAH clusters was far from trivial[60]). The intermolecular vibrational modes lying in the far-IR range, and which are not a priori expected to depend significantly on the intramolecular modes, can be calculated using V_{inter} with rigid coronene molecules. The various isomers and the disordered phase of coronene clusters are also more conveniently sampled using the intermolecular potential only. The way of incorporating intramolecular modes in the thermodynamic properties will be described in section IV.

III. Vibrations of Coronene Clusters

A. Methods. The complete vibrational frequencies of coronene clusters have been obtained at the harmonic level, by diagonalizing the dynamical matrix (that is the mass-weighted Hessian matrix) K_{ij} on the total Hamiltonian including intermolecular and internal modes, at the global minimum geometry:

$$K_{ij} = \frac{1}{\sqrt{m_i m_j}} \frac{\partial^2 H_{\text{total}}}{\partial q_i \partial q_j} \tag{3}$$

Here q_i denotes any Cartesian coordinate. For a cluster having N_{mol} molecules, each containing N_{at} atoms ($N_{\text{at}} = 36$ for coronene), **K** is a square matrix with dimension $n_{\text{modes}} = 3N_{\text{mol}} \times N_{\text{at}}$. The diagonalization of matrix **K** provides n_{modes} eigenvalues, among which six zero-frequency modes correspond to the overall translation and rotation modes. The eigenvector of mode l is denoted as $\mathbf{u}_l$.

The cluster structure used for the Hessian calculation was locally optimized from the cluster geometry obtained with the pure intermolecular potential V_{inter} with the molecules assumed to be rigid.[60] The PAH molecules undergo barely noticeable rearrangements upon releasing the internal degrees of freedom. In practice, the dynamical matrix was calculated by numerical differentiation of the first-order derivatives obtained analytically thanks to the Hellmann−Feynman theorem.

The contribution of the intermolecular modes to the global motion of mode l on the H_{total} energy surface was determined by projecting the eigenvector $\mathbf{u}_l$ onto the vectors of a basis able to span uniquely the intermolecular modes. These modes consist of $3N_{\text{mol}}$ translations and as many rotations, considered for the stable cluster structure in which all individual molecules are treated as rigid (without sharing the same geometry). A suitable basis for translations is built by considering the individual translations $\mathbf{t}_{i\alpha}$ of molecule i along the $\alpha = x, y, z$ axes. Similarly a basis $\mathbf{s}_{j\theta}$ for rotations around the axes $\theta = x, y, z$ of molecule j is built, the infinitesimal rotation of atom k being written as $\mathbf{e}_\theta \times (\mathbf{r}_{jk} - \mathbf{r}_j^{\text{com}})$. In this equation $\mathbf{e}_\theta$ is the unitary vector of axis θ, $\mathbf{r}_{jk}$ is the position of atom k of molecule j, and $\mathbf{r}_j^{\text{com}}$ is the position of the center of mass of molecule j. The set of $6N_{\text{mol}}$ vectors **t** and **s** already forms an orthogonal basis, and we further normalize it into the $\{w_k, k = 1, ..., 6N_{\text{mol}}\}$ set, distinguishing the translation and rotation components by (t) and (r) superscripts, respectively. The projection of the vector $\mathbf{u}_l$ onto the basis $\mathbf{w}_k$ yields the vector $\mathbf{u}_l^{\text{inter}}$ and introduces some coefficients $c_{kl}^{(t)}$ and $c_{kl}^{(r)}$ as

$$\mathbf{u}_l^{\text{inter}} = \sum_k c_{kl}^{(t)} \mathbf{w}_k^{(t)} + \sum_{k'} c_{k'l}^{(r)} \mathbf{w}_{k'}^{(r)} \tag{4}$$

The weights $W_l^{(t)}$ and $W_l^{(r)}$ of intermolecular translation and rotation of normal mode l are then expressed as

$$W_l^{(t)} = \sum_k [c_{kl}^{(t)}]^2,\ W_l^{(r)} = \sum_{k'} [c_{k'l}^{(r)}]^2 \qquad (5)$$

whereas the global intermolecular weight of mode l is $W_l^{(t)} + W_l^{(r)}$. These numbers are discussed more easily in terms of percentages. Projecting the cluster vibrational modes obtained with the full Hamiltonian H_{total} onto the intramolecular modes is also possible, by rotating the eigenmodes of the isolated coronene molecule in the reference frame of each molecule in the cluster. Such a projection was performed for the dimer in order to identify the intramolecular modes and their splitting upon clustering.

We also calculated the vibrational frequencies of the purely intermolecular potential V_{inter}, using global coordinates for the PAH molecules. Initial attempts with the Euler angles were found to be rather unstable,[71] and we used the coordinate system proposed by Murry and co-workers[71] to get rid of the instability. The results were checked using the OPTIM program[72] which uses a single unitary vector rigidly fixed to the molecular frame as the orientational degrees of freedom.[73]

Before showing and discussing the results, we should emphasize that we focus here on the vibrational frequencies, but that we have not calculated the IR intensities. The TB model used in the present work predicts relative intensities from the second derivatives of the dipole moment that differ from those observed experimentally or calculated by *ab initio* methods.[74] This is likely due to the imperfect description of charge transfer within the TB model, which directly affects the dipole moment. Therefore, we have not attempted to include intensities here, in order to avoid spurious artifacts and misinterpretations of the results.

B. Mid-Infrared Range. We first analyze the influence of aggregation on the vibrational modes with above 50 wavenumbers, a value which is comparable to the softest mode in the coronene molecule (about 90 cm^{-1}, see Table 1). Depending on whether their frequency is lower or higher than 300 cm^{-1}, modes will be denoted as "soft'' or "hard'', respectively. The mid-infrared part of the vibrational spectra of coronene clusters containing $N_{\text{mol}} = 2$, 4, or 8 molecules is represented in Figure 1. The spectrum of the single $C_{24}H_{12}$ molecule is also shown for comparison. While the dimer and tetramer are single-stack structures, the octamer has a handshake-like structure formed by two four-stack next to each other.

As can be seen from Figure 1, the soft modes are strongly affected by aggregation, and the dispersion of the new frequencies is particularly clear in the 80−200 cm^{-1} range. However, the effects differ notably between the single- and double-stack structures. In a one-dimensional stack of N_{mol} molecules, and for any given internal mode k of the isolated coronene molecule, a series of cluster modes emerge from a combination of this molecular mode, each mode corresponding to individual molecules vibrating with different phases. At least one of these modes stays close to the frequency of the original mode k, whereas the others are shifted toward higher wavenumbers. This phenomenon is illustrated in the lower panel of Figure 1 on the specific case of the "bowl'' mode, located at 130.5 cm^{-1} in gas-phase coronene. Two similar bowl modes are found in the coronene dimer, in which the individual molecules vibrate in-phase (case a, also denoted as − − or + +) or out-of-phase (case b, also denoted as − + or + −). In the in-phase case, the distance between the centers of mass of the two molecules remains approximately constant during the vibrational motion, and the relative orientations of the molecules are fixed. The distances between atoms of two molecules do not strongly vary during the motion; hence, the intermolecular energy is not affected significantly. This explains why the corresponding cluster mode is also found very close to 130.5 cm^{-1}.

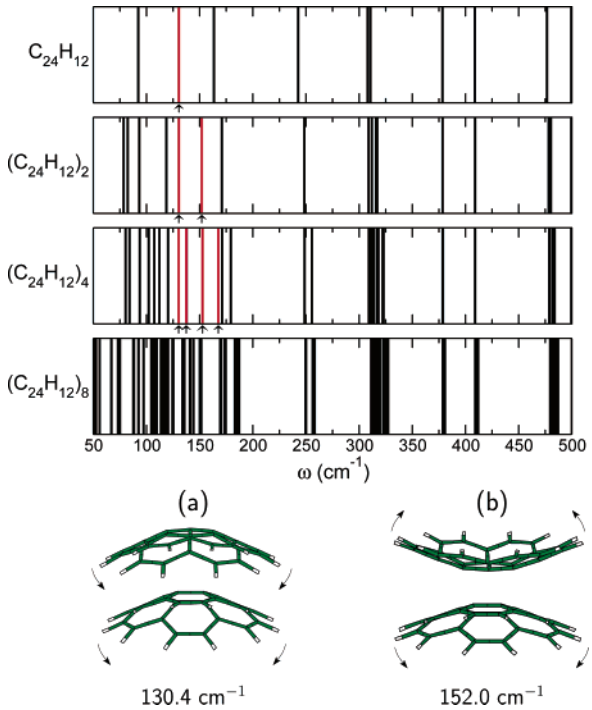

Figure 1. Vibrational spectra of small $(C_{24}H_{12})_n$ clusters in their global minimum structure, for $n = 1$, 2, 4, and 8, in the 50−500 cm^{-1} range. The purely intramolecular "bowl'' modes are highlighted in red and marked with small arrows. In parts a and b, the two bowl modes of the dimer, associated with the patterns − − and − +, respectively, are illustrated along with their frequencies.

Conversely, the out-of-phase bowl mode depicted in Figure 1 involves a rather strong change in the pairs of atoms belonging to either molecule, resulting in a nonnegligible contribution of the intermolecular energy. In addition, the distance to the equilibrium cluster geometry is larger for the out-of-phase mode, leading to harder vibrations, consistently with the higher frequency calculated for this mode, at 152.0 cm^{-1}.

More generally, by projecting the vibrational mode obtained from the total Hamiltonian on the vibrational modes of the single coronene molecule, one can identify the in-phase and out-of-phase molecular modes corresponding to each intramolecular mode. In the tetramer, the bowl mode with all molecules vibrating in-phase lies at 130.3 cm^{-1} and is again marginally affected by the intermolecular energy. Other bowl modes corresponding to different dephasing of the molecules are also shifted to higher frequencies, the shift being more important if neighboring molecules are out-of-phase. The − − ++, − ++ −, and − + − + patterns, associated with the frequencies of 137.4, 152.7, and 167.6 wavenumbers, respectively, are highlighted in Figure 1 as small arrows. As the number of molecules in the stack increases, the combination of bowl modes will broaden, with higher and higher frequencies.

Such shifts are not limited to the specific bowl mode, and are observed on the other soft modes. However, the contribution of the intermolecular energy on the magnitude of the shift will depend on the nature of the internal mode. For the stacked dimer, each vibrational mode is split into two cluster vibrational modes, one in-phase and one out-of-phase, respectively, each having a specific frequency. The relative shift of the cluster mode with respect to the original intramolecular mode can then be calculated for all the $3N_{\text{at}} - 6 = 102$ internal modes, as

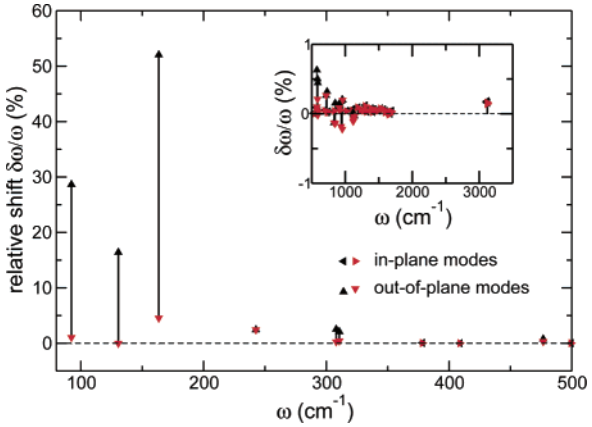

Figure 2. Relative variations in the vibration frequency upon stacking together two coronene molecules, as a function of the initial frequency in the single molecule. The upper and lower values are labeled in black and red symbols, and the out-of-plane and in-plane vibrational modes are distinguished. The inset highlights the 500−3500 cm^{-1} range.

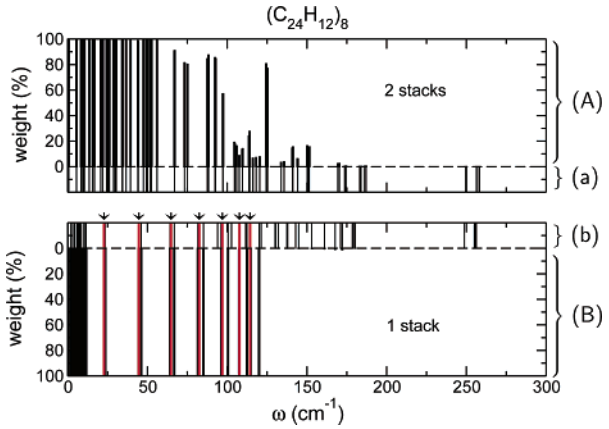

Figure 3. Vibrational spectra of the $(C_{24}H_{12})_8$ cluster, in its 2-stack global minimum [(a and A), upper panel] or as a 1-stack [(b and B), lower panel]. The entire spectra are shown in the (a and b) minor parts of the panels, while the contributions of intermolecular modes, obtained by projecting the initial eigenvectors, are given (in percents) in the (A and B) major parts of the panels. For the 1-stack structure, the linear modes are also superimposed as red bars, and highlighted with arrows.

represented in Figure 2. In this figure, we distinguished between intramolecular modes corresponding to motions in the plane of the coronene molecule, denoted as "in-plane'', and out-of-plane modes for which the eigenvector has an important component perpendicularly to the coronene plane.

Figure 2 shows that the soft modes can undergo very strong vibrational shifts due to aggregation, up to 50%. In general, the shift is smaller for harder modes. The hard modes involving direct C−C or C−H vibrations (located below approximately 600 cm^{-1}) exhibit practically no shift (less than 1%), as seen on the inset of Figure 2. This graph, as well as other calculations on coronene clusters containing up to 16 molecules, indicate that the hard modes are poorly sensitive to clustering in itself, and to the structure of the cluster either, at the present harmonic level of approximation. The band shift was found to be smaller than 1% for modes having a frequency above 600 wavenumbers.

In the case of the dimer, the modes that are mainly affected are also those involving out-of-plane motion, even if they lie in the same frequency range as in-plane modes (e.g., near 200−500 cm^{-1}). Obviously, this correlation is not fortuitous. As analyzed above for the specific bowl mode, the shift in frequency is due to the contribution of intermolecular energy. While in-plane modes are not significantly affected by this energy, out-of-plane modes are generally hindered by the presence of the other molecule, hence resulting in a blue shift. Therefore, in the case of the single-stack clusters, the modes that are the most affected by aggregation are those involving out-of-plane soft modes.

The previous analysis is specific to the smaller clusters, more stable as a single stack, and for which the intermolecular and intramolecular modes are only weakly coupled. In particular, the single-molecule modes can be clearly identified on the cluster modes. We have decomposed all modes of the two-stack coronene octamer into translation, rotation, and pure intramolecular contributions, following the procedure described in section III.A. The weights of the global intermolecular modes (translation + rotation) on the cluster modes are represented as a function of the frequency in Figure 3. The same decomposition, for the single-stack isomer of the octamer, is also shown on the lower panel of this figure. For clarity, small portions of the graphs contain the full spectra.

As previously noticed on the dimer, all vibrational modes of the single-stack isomer of the octamer are nearly perfectly decoupled in terms of their intermolecular and internal contributions, the corresponding weights being always in the 0−1% or 99−100% ranges. On the contrary, the two types of modes can mix significantly in the two-stack, global minimum structure. Below 60 cm^{-1}, the softer cluster modes are purely intermolecular in nature. Above 200 wavenumbers, on the other hand, the hard modes are purely intramolecular. In the intermediate range, the degree of mixing is important, but not necessarily monotonic with the frequency, or hardness, of the mode. In this range, the softest internal modes of the coronene molecule within a stack are strongly constrained by the molecules in the neighboring stack. This is also true for the global rotations and translations of a molecule in a stack, which rubs against the other stack.

The combination of inner- and intermolecular vibrations leads to an important strain experienced by the molecular skeleton of the individual coronene molecule, as depicted in Figure 4 for four typical modes in the intermediate mixing range.

The snapshots for the two modes with a high intermolecular component (one consisting of 57% rotations and one consisting of 60% translations and 21% rotations) illustrate the rather small deformations sustained by the molecules. The two modes with a high intramolecular content deviate more strongly from the flat, equilibrium geometry of coronene.

While Figure 1 compared vibrational spectra for clusters having different sizes, Figure 3 emphasizes the dispersion in the spectra due to the nonstacking effect, at a same given size. The vibrations of the single-stack isomer of the coronene octamer can be compared to the simple 1D model of Seahra and Duley, who studied the discrete dispersion relation for stack vibrations.[62] For a stack of N_{mol} molecules the N_{mol} vibrational frequencies along the stack axis are expressed as

$$\omega_i^{stack} = \omega_0\sqrt{2}\sin\left[\frac{\pi(i-1)}{N_{mol}}\right], \quad i = 1, ..., N_{mol} \qquad (6)$$

where $\omega_0 = 82.4$ cm^{-1} is the frequency of the dimer breathing mode.[60] Among the 8 values calculated for the octamer, one is zero, corresponding to the global translation. The remaining seven modes are highlighted as small arrows on the lower panel of Figure 3.

The stack vibration modes of the coronene octamer are well reproduced by the above formula. However, around each value of ω_i^{stack}, there are many other modes corresponding to the

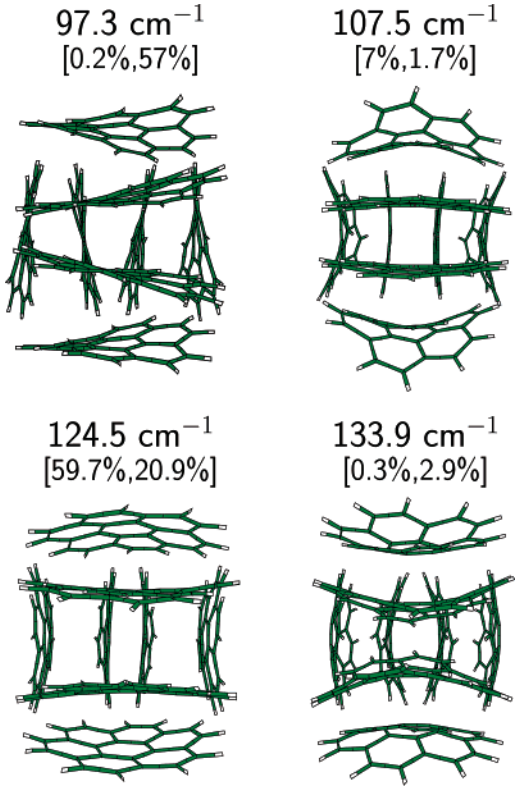

Figure 4. Illustration of some vibrational modes of $(C_{24}H_{12})_8$ with various internal and intermolecular contributions. Each mode is identified by its frequency, and the respective weights of translations and rotations, respectively, are given between brackets as $[W^{(t)},W^{(r)}]$. The missing contribution of intramolecular modes complements 10%.

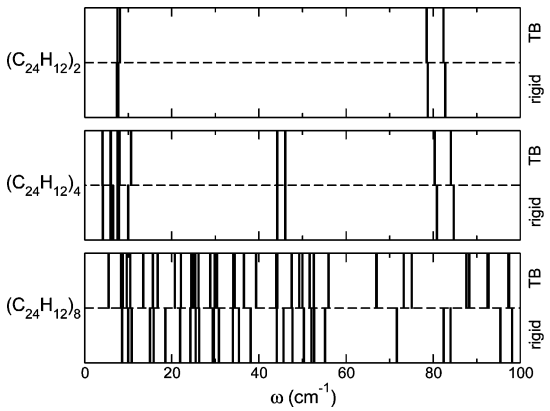

Figure 5. Vibrational spectra of $(C_{24}H_{12})_n$, $n = 2$, 4, and 8, in the far-IR range below 100 wavenumbers. For each cluster, the spectra obtained by considering either the full Hamiltonian or by treating each molecule as rigid are shown in the upper and lower half of the panels, respectively.

combinations of the bending mode ω_0^{bend} (twofold degenerated) into the set of 14 extra modes ω_i^{bend}, each slightly below ω_i^{stack}. Other purely intermolecular modes are discussed in the next section.

C. Far-Infrared Spectrum. We now turn to the far-IR modes with frequencies below 100 cm^{-1}. The spectra of these modes obtained using either the total intermolecular + internal Hamiltonian or the V_{inter} potential alone with rigid $C_{24}H_{12}$ molecules are represented on Figure 5 for the dimer, tetramer, and octamer. The main difference between the dimer and the tetramer lies in the presence of very soft modes (4.06, 5.86 × 2, 6.03, and 6.05 cm^{-1}) in the latter. These modes correspond to collective deformations of the stack. For instance, the global twisting mode occurs at 4.06 wavenumbers in the tetramer, but at twice this frequency in the dimer. More generally, single-stack structures will exhibit softer and softer modes as the stack size increases. As the one-stack motif no longer competes with more compact structures (for coronene, that means above seven molecules), the vibrational modes should become significantly harder.

The collective deformation of the stacks are significantly hindered in the two-stack structure of the octamer, which leads to an important hardening of the intermolecular modes, as manifested by a general increase in the frequency. The softest mode in the two-stack structure of the octamer is found at 5.45 cm^{-1}, and at 1.8 cm^{-1} only in the single-stack isomer. This large difference can be interpreted by looking at the respective contributions of the internal and intermolecular energies, following the corresponding eigenvector. Using the total Hamiltonian, the intramolecular energy is seen to be *maximum* at the cluster equilibrium geometry, whereas the total potential energy is (correctly) a minimum. The intramolecular contribution softens the mainly intermolecular mode, which shifts its frequency toward lower values. This phenomenon can be somewhat seen as the opposite of the shift exhibited by the intramolecular modes upon including the intermolecular contribution.

The two-stack structure of $(C_{24}H_{12})_8$ is also at the origin of strong couplings between intermolecular modes. In the dimer, intermolecular modes can be divided in two groups, the hardest bending and breathing modes being around 80 cm^{-1}, while the soft twisting and shearing modes lie near 8 wavenumbers.[75] In single stacks, these modes combine together into collective vibrations, with frequencies given by formulas similar to eq 6. The cluster modes are in general marginally affected by the internal degrees of freedom. As seen from Figure 5, assuming the molecules to be rigid does not change the frequency of the corresponding mode by more than 5%. This is no longer true for the two-stack octamer, where the frequency of only few cluster modes can be identified by the purely intermolecular modes obtained with the rigid molecule assumption. The 8−80 cm^{-1} spectral range, which is rather sparse for the single-stack isomer, is filled in the two-stack structure due to two related effects. The first direct effect is the frustration experienced by the collective, single-stack modes due to the presence of the other stack, as illustrated in Figure 4 on the 124.5 cm^{-1} mode. The accumulation of harder intermolecular modes above 20 wavenumbers due to the specific, two-stack structure is clearly seen on the rigid modes. There is an additional, indirect effect of clustering on the vibrational spectrum. As shown by the difference between cluster modes calculated using all degrees of freedom and those on the V_{inter} surface with rigid molecules, the geometry relaxation of individual molecules upon aggregation is significant, while it is negligible for single stacks. Another hint that geometry relaxation affects the intermolecular modes is the generally higher frequencies of the rigid modes, with respect to the cluster modes obtained with all degrees of freedom. Therefore, small differences in geometry have important consequences on the softest vibrations.

The above study, as well as the previous discussion on the mid-IR range, indicate that the couplings between intermolecular and internal modes are strong for multiple-stack structures. In particular, the assumption that collective modes arise from one-dimensional, single-stack conformations is clearly too simplistic. Our results show that bunches of cluster modes arise from aggregation of coronene molecules into multiple stacks, and that the geometrical strain significantly hardens the modes.

IV. Caloric Curves

A. Methods. The previous section was devoted to vibrational properties at the harmonic level. We now seek to characterize the finite temperature behavior of coronene clusters. The direct simulation by Monte Carlo or molecular dynamics methods using the full quantum/classical Hamiltonian is not conceivable, essentially due to the relatively heavy numerical cost of the TB model, to the need for a significant (ergodic) sampling of the energy surface, but also the different magnitudes of atomic and molecular motion. In order to sample the structural isomerization in the cluster, we first performed Monte Carlo simulations on the electronic ground state H_{inter} potential energy surface, assuming frozen coronene molecules. These simulations were improved with the all-exchange parallel tempering strategy[76] using a geometric distribution of 50 temperatures in the 10−1000 K range. For each replica, 10^6 MC cycles were carried out following 5×10^5 equilibration cycles. To prevent thermal evaporation at high temperatures, the cluster was confined into a hard-wall spherical container, all configurations with a molecule distant by more than 8 Å from the center of mass being rejected from the statistics in the propagation of the Markov chain. The molecular orientations were described in terms of quaternion coordinates. From the distributions of potential energies, a multiple histogram reweighting procedure provided the classical microcanonical density of states and, after Laplace transformation, the anharmonic partition function $Z^{a,c}_{\text{inter}}$ as a function of temperature.

Even though the frequencies are coupled between inter- and intramolecular contributions, we assume that the internal modes do not play an important role on the structural transitions, which are primarily driven by isomerizations on the intermolecular potential energy surface. Under this approximation the total, classical partition function $Z^{a,c}_{\text{total}}$ of the cluster is obtained by factorizing the inter- and intramolecular contributions as

$$Z^{a,c}_{\text{total}}(T) \simeq Z^{a,c}_{\text{inter}}(T) \times [Z^{a,c}_{\text{intra}}(T)]^{N_{\text{mol}}} \tag{7}$$

The anharmonic partition function $Z^{a,c}_{\text{intra}}$ of the isolated coronene molecule was calculated also from the distributions of potential energies gathered during Monte Carlo simulations, processed with histogram reweighting. A total of 20 trajectories were carried out at temperatures in the 5−1000 K temperature range, with 10^5 atomic steps per trajectory, the first 30% being discarded for equilibration. Below 1000 K, regular deformations and anharmonicities were found, the variations of the classical heat capacity with temperature being essentially linear with a small positive slope (about 10^{-3} k_B/K). This indicates that $Z^{a,c}_{\text{intra}}(T)$ deviates only moderately from the harmonic behavior, which could be expected from the small number of soft modes in coronene with respect to the total number of modes. We thus write

$$Z^{a,c}_{\text{intra}}(T) \simeq \frac{1}{24}\left(\frac{k_B T}{\hbar\bar{\omega}}\right)^{3N_{\text{at}}-6} \tag{8}$$

where $\bar{\omega}$ is the geometric average of the vibrational frequency of the coronene molecule (926 cm^{-1} with the present TB model), and the prefactor 1/24 accounts for the D_{6h} symmetry.

Quantum vibrational effects were included using the Pitzer−Gwinn (PG) approximation.[69,77] In this approach, the quantum anharmonic partition function $Z^{a,q}_{\text{total}}(T)$ is the product of its classical counterpart $Z^{a,c}_{\text{total}}(T)$ by a quantum/classical correcting factor corresponding to the same system, but treated at the harmonic level:

$$Z^{a,q}_{\text{total}}(T) \simeq Z^{a,c}_{\text{total}}(T) \times \frac{Z^{h,q}_{\text{total}}(T)}{Z^{h,c}_{\text{total}}(T)} \tag{9}$$

In this equation, $Z^{h,q}_{\text{total}}/Z^{h,c}_{\text{total}}$ is the ratio of the harmonic partition functions calculated for quantum and classical oscillators, respectively, taking inter- and intramolecular modes of the ground state structure into account.

From the variations of the partition function, the canonical heat capacity was obtained by numerical derivatives. To interpret the caloric curve, the configurations from the MC trajectories were periodically quenched. This method provides a connection with the energy landscape associated with the H_{inter} potential. The quenches were performed with an adaptive stepsize steepest descent local optimizer.

B. Results. The classical ($\hbar = 0$) and quantum heat capacities of $(C_{24}H_{12})_8$ are shown in Figure 6.

In the quantum case, in addition to the reference curve for which vibrational delocalization is exactly quantified by the Planck constant, two other calculations are represented, corresponding to intermediate but artificial regimes where $\hbar/5$ and $\hbar/10$ are used instead of $\hbar$. These extra curves illustrate how quantum effects contribute to the overall shape of the heat capacity.

The classical cluster exhibits a broad heat capacity peak at low temperatures $T \sim 50$ −300 K, but the number of degrees of freedom that contribute actively to the heat capacity ($6N_{\text{mol}} - 6 = 42$) is very small compared to the entire number of modes ($3N_{\text{mol}}N_{\text{at}} - 6 = 858$). This explains why the peak in the classical curve only marginally exceeds the Dulong−Petit limit.

As quantum delocalization is switched on, the heat capacity recovers the expected behavior, and vanishes as T goes to zero. At $\hbar/10$ delocalization already extends significantly up to 200 K, removing all signatures of the bump in the classical curve. As the Planck constant recovers its physical value, the variations in the heat capacity become notably flat, consistently with the strong internal modes of coronene. At the transition temperature, the coronene molecules are all strongly rigid and frozen, confirming our hypothesis that the thermodynamics of coronene clusters can be separated into its internal and intermolecular contributions. This also further supports the conclusions reached by Schmidt et al.,[59] that coronene clusters are extremely heterogeneous also from the thermodynamics point of view.

Even though the magnitude of quantum effects is large enough to hide all features in the classical caloric curve, the underlying phenomena that are responsible for the bump in the heat capacity are intrinsic to the cluster, and are not expected here to depend significantly on its classical or quantum nature. The spectra of isomers obtained from periodically quenching 1000 configurations are represented in Figure 7 against the replica temperature in the MC simulations. Some typical structures found during these quenches, including the global minimum itself, are illustrated in Figure 8.

As temperature remains below approximately 100 K, a large number of isomers appears with energies slightly higher than the global minimum, in the range -700 kcal/mol $\leq E \leq -690$ kcal/mol. Visual inspection reveals that all these isomers are actually based on the same double stack, 4 + 4 motif as the ground state structure, except that they differ slightly by a shift and/or a twist in one or more molecules. The B isomer of Figure 8, for instance, has all molecules in each stack still parallel, but the molecular sixfold axes are no longer aligned with the stack axes. The multiple 4 + 4 double stack structures indicate a strong geometric frustration associated with the competition between inter- and intra-stack interactions. The sharp increase

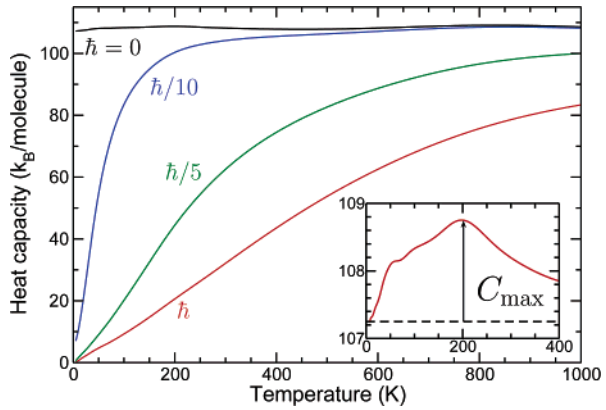

Figure 6. Canonical heat capacity of the $(C_{24}H_{12})_8$ cluster obtained from classical simulations, and corrected for quantum effects using the Pitzer−Gwinn approximation, for various values of the Planck constant, including the normal physical value $\hbar$ as well as reduced, artificial values $\hbar/5$ and $\hbar/10$. The inset shows the classical result, as well as the Dulong−Petit curve as an horizontal dashed line.

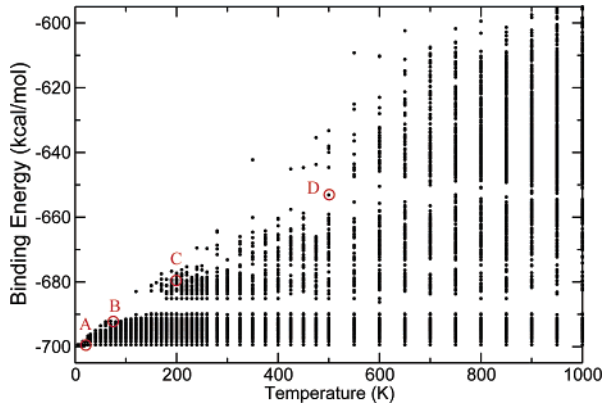

Figure 7. Energies of $(C_{24}H_{12})_8$ isomers obtained from quenching Monte Carlo trajectories, as a function of the replica temperature. Four isomers are emphasized in red.

in the classical heat capacity, seen in the inset of Figure 6 below about 50 K, is thus the consequence of the many new, nearly degenerate isomers that can be accessed even at low temperatures.

As T reaches 200 K, a new band of structures arises, an example being offered as isomer C in Figure 8. The rearrangements needed to break one stack, leading to the 5 + 3 structure, are more significant than those involved in twisting or shifting around the 4 + 4 global minimum. This explains the small but clearly visible energy gap in the range -690 kcal/mol $\leq E \leq -685$ kcal/mol in Figure 7. The peak in the classical heat capacity near $T = 200$ K, which we interpret as the signature of the melting phase change, is thus correlated with the thermal instability of the stack units. Interestingly, the melting temperature found here for 8 molecules lies notably below the melting temperature of bulk coronene of 710.5 K.[67,68] This strong reduction in the melting point is the trend expected for such small systems.

At temperatures higher than 300 K many isomers appear, usually with even shorter stacks and possibly single molecules not directly part of a stack. Isomer D of Figure 8, with energy -653.27 kcal/mol, consists of a 4 + 2 + 2 triple stack structure.

The above results show that, even though the caloric curves do not display sharply resolved variations, many isomers and structural transitions take place in coronene clusters at temperatures as low as 100 K or even less. Because they are all based on the same 4 + 4 two-stack motif, the isomers sampled at low temperatures are likely to be separated by low-energy barriers, and a relatively fast relaxation kinetics is expected. Breaking a stack, on the other hand, should involve much higher barriers and longer rearrangements, being thus also much slower.

On the basis of our findings the thermodynamical behavior of larger PAH clusters can also be inferred, at least qualitatively. As the number of PAH molecules in the cluster increases, the heat capacity peak should become higher and narrower, and shifted to higher temperatures. Conversely, quantum delocalization does not vary much with the number of molecules. Hence, above some critical size the melting peak should become visible on the quantum caloric curve. Our results suggest that $N_{mol} = 8$ molecules are far below this limit. More precisely, a simple model can reasonably account for the observed behavior and allow a semiquantitative prediction of the crossover size above which the melting transition could be detected on the quantum caloric curve.

We will assume that the solid−liquid phase change is a first-order transition rounded by size effects, which seems quite reasonable for such molecular clusters.[78] The idea consists of writing eq 9 differently, by considering the harmonic quantum state as the reference and the ratio involving only the classical partition functions as the correction. For clarity we now denote as N the number of molecules in the cluster. The melting phase change occurs as a finite peak on the heat capacity $\Delta C_v(T,N)$, which is an additional contribution to the normal, Dulong−Petit part $C_v^{h,c}(T, N) = (6N - 6)k_B$. A two-state approximation for the partition function[79] leads to a Gaussian expression for $\Delta C_v(T,N)$ as

$$\Delta C_v(T,N) \approx C_{max}(N) \exp\left[-\left(\frac{T - T^*(N)}{\Delta T(N)}\right)^2\right] \qquad (10)$$

where $T^*(N)$ is the center of the peak, that is the melting temperature of the cluster, and $\Delta T(N)$ is the width of the transition. $C_{max}(N)$ marks the top of the peak, shown in the inset of Figure 6. For a first-order transition, $T^*(N)$ is expected to increase roughly with the inverse radius of the cluster,[80] and we write

$$T^*(N) \approx T^*(\infty) - \frac{T_0}{N^{1/3}} \qquad (11)$$

where $T^*(\infty) = 710.5$ K is the bulk melting temperature,[67,68] and T_0 a parameter. Similarly, and following Imry,[81] the width of the transition scales with size as

$$\Delta T(N) \approx \frac{\delta T}{N} \qquad (12)$$

with δT another parameter. The value of the heat capacity at the melting point, normalized by the number of molecules, $\Delta C_v[T^*(N)]/N = C_{max}(N)/N$, controls whether the peak can be distinguished from the main contribution to the heat capacity due to the quantum vibrational modes of coronene, $C_v^{h,q}[T^*(N)]$. Assuming that the latent heat of fusion does not vary significantly with the number of molecules, $C_{max}(N)$ is found to be proportional to N^2, in agreement with Berry and Smirnov,[79] and we write $C_{max}(N) \approx aN^2$. Therefore, as N increases, the heat capacity peak becomes narrower and sharper, as expected for a first-order transition. Above some crossover size N^* it becomes comparable to the intramolecular contribution $C_v^{h,q}$, which is essentially constant with N, and thus noticeable. The crossover N^* is defined such that the peak in the heat capacity has the same order of magnitude of the intramolecular heat capacity, or

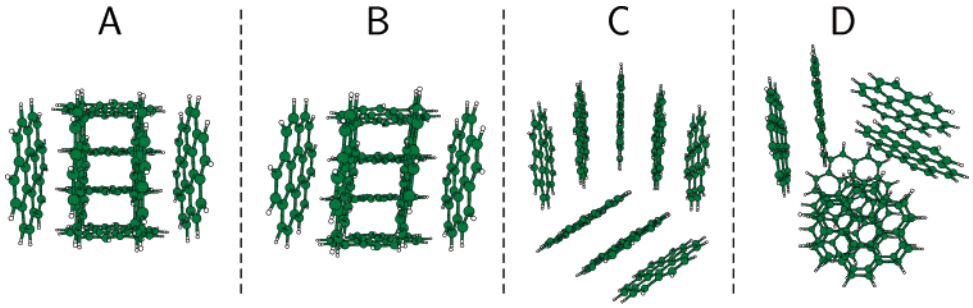

Figure 8. Typical isomers of $(C_{24}H_{12})_8$ labeled as A, B, C, and D in Figure 7. The global minimum is structure A.

$$\frac{C_{\max}(N^*)}{N^*} = aN^* \sim C_v^{h,q}\left[T^*(\infty) - \frac{T_0}{(N^*)^{1/3}}\right] \qquad (13)$$

The above simple model has only two free parameters, namely T_0 and a, which are fixed by the caloric curve obtained for the octamer. We find $T_0 = 1021$ K and $a = 0.1875k_B$. Solving numerically eq 13 with these values leads to $N^* \sim 300$ molecules. This relatively large number is consistent with the rather small latent heat of fusion (0.2 eV) of bulk coronene, which is barely noticeable on the caloric curve.[59]

While melting in large coronene clusters may involve complex, and possibly competing interstack and intrastack melting mechanisms, the general picture could be reasonably well described by the present example of the octamer. Large amplitude, global vibrations will first lead to a variety of multiple stack isomers built around the ground state structure. The onset of solid−liquid phase change should then occur with the breaking and re-formation of stacks, leading to new classes of isomers.

Here we have not explored the dynamical aspects of melting. In the realistic situation of a gas-phase cluster without an artificial container around it, the rearrangements involved during melting, together with the rather short range of the intermolecular interaction, will probably favor thermal dissociation. This is supported by the low boiling temperature of bulk coronene, only about 10% higher than the melting point.[67,68] Hence, and as in the case of C_{60} (refs 82 and 83), it is unclear whether the liquid phase of coronene clusters will be stable, and what the typical lifetimes of this phase could be.

Above 1000 K coronene clusters will undergo multiple rearrangements before thermally dissociating. The molecules themselves should become more and more floppy, and bond breaking is expected above around 2000 K. At such high temperatures, neutral PAH clusters should not survive for very long times.

V. Conclusion

Fully coordinated polycyclic aromatic hydrocarbons can form clusters in which the molecules are stacked in a one-dimensional way along the same axis, or as intertwined shorter stacks for larger clusters. PAH clusters are characterized by a strong disparity between the inner covalent forces and the intermolecular, dispersion and electrostatic interactions. In the present paper, we theoretically investigated the vibrational spectra of coronene clusters, using a quantum/classical atomistic model combining a tight-binding Hamiltonian fitted to reproduce first-principle data on isolated PAHs[63] with an explicit site−site pairwise potential[60] to describe intermolecular bonding. The normal modes of the most stable structures of $(C_{24}H_{12})_n$ clusters containing up to 8 molecules have been obtained at the harmonic level. By comparing the results with the spectrum of the gas-phase coronene molecule, we paid a particular attention to the aggregation effects.

From a general point of view, the present model does not lead to important variations in the frequencies of the hardest infrared modes lying above 500 wavenumbers. Conversely, the soft modes in the mid-IR range (80−300 cm^{-1}) exhibit significant shifts. By projecting the vibrational eigenvectors onto restricted bases of purely intermolecular or internal modes, we have shown that the vibrations of singly stacked clusters are fully decoupled between those modes. Upon clustering the soft internal modes are splitted into in-phase and out-of-phase collective modes, the latter being significantly harder. Looking more closely at the dimer, we also obtained the intuitive result that individual modes having a component perpendicular to the molecular plane are more prone to being shifted upon clustering. For the two-stack octamer cluster, the internal and intermolecular modes mix in the mid-infrared range. Because of the geometric strain experienced by the molecules in their rubbing motion against the other stack, the vibrational modes are much harder than in the linear, single-stack isomer.

The far-IR part of the spectra also varies depending on cluster structure. In single-stack clusters, the breathing or bending modes of the coronene dimer combine into collective modes that essentially follow the standard dispersion relations of one-dimensional chains, and are located sparsely in the 20−100 cm^{-1} range. In the two-stack geometry, the intermolecular modes of the octamer mix with inner modes, filling this range. Moreover, the purely intermolecular vibrational frequencies obtained by freezing the molecules in their gas-phase geometry underestimate the frequencies of the actual cluster modes. This suggests that the distortions experienced by the PAHs in the cluster, albeit small, have manifestations on the softer modes.

We also investigated the finite-temperature behavior of the coronene octamer. The classical, anharmonic partition function was calculated as a function of temperature by performing classical exchange Monte Carlo simulations on the intermolecular energy surface. Here the frozen approximation is used to sample the various isomer configurations, avoiding the extra numerical cost of the TB model. Quantum effects were added a posteriori, using the Pitzer−Gwinn semiclassical approximation. The much stronger intramolecular bonds were seen to damp the heat capacity by significant amounts, hiding the possible effects of a solid−liquid transition rounded by size effects. Assuming that the transition is of the first-order type, we predicted from a simple two-state model that several hundred molecules should be necessary for the melting peak to be visible. Even though the caloric curve is blurred by delocalization effects, structural transitions take place indeed, as evidenced on the spectra of isomers obtained from periodically quenching configurations. The global minimum, two-stack structure of the

cluster was seen to be rather soft, many isomers being found upon shifting or twisting the molecules by a small amount. At the heat capacity peak occurring near 200 K, the stacks break, and new isomers based on the 5 + 3 motif appear. At higher temperatures, the typical isomers consist of three or more shorter stacks, or even molecules that do not belong to any stack.

The present work was limited to the case of homogeneous and neutral coronene clusters, which are typical PAHs with a reasonable size. Clusters of other molecules could be of course investigated as well, but the high symmetry of coronene significantly simplifies the problem in reducing the number of vibrational modes. Heterogeneous clusters could be also studied using the same combined Hamiltonian, but the mixing of modes should be also much more important. Two other limitations are the relative intensities of the vibrational modes, as well as anharmonicities. While our atomistic model can account for the frequency shifts, the TB part does not correctly reproduce the intensities obtained from more sophisticated DFT data on the gas-phase molecule.[74] As far as static calculations are concerned, upgrading the TB model to a DFT-like level would probably improve the situation. At the expense of a new parametrization, it would then be possible to predict relative intensities, and look more closely at the clustering effects on the infrared spectra. Another possibility for estimating the intensities would be to use the density-functional based tight-binding method.[84,85] This would be especially valuable in the mid-IR region where the modes are not shifted significantly, but the intensities may be affected.

Anharmonicities could be incorporated by performing molecular dynamics simulations on the ground state energy surface of the H_{total} Hamiltonian, using appropriate Fourier transform of the square dipole moment. The identification of the modes, however, remains a problem for such brute-force methods, and it would be interesting to implement recent schemes such as the one recently proposed by Martinez and co-workers[86] in this purpose.

From the experimental point of view, the present work indicates that PAH clusters would be better characterized from the vibrational spectra in the far-IR range, rather than the mid-IR range. In the context of astrochemistry, where PAH clusters are plausible candidates as precursors of free-flying PAH molecules in the interstellar medium, this work shows that PAH clusters are good candidates to account for the low frequencies features. In particular, they could be evidenced by forthcoming space observatories such as Herschel and its 16−175 cm^{-1} probing range. The neutral coronene clusters investigated here are an oversimplified representation of actual aggregates with various polycyclic aromatic molecules and various charge states. PAHs are likely to carry a charge in the interstellar medium.[16,87] Anions are likely to emit their electrons by photodetachment in irradiated regions. Multiply charged molecules should be less stable due to Coulomb repulsion, and will not form clusters. Cationic PAHs, on the other hand, may be particularly stable. In the case of clusters, the single positive charge should lead to a significant stabilization with respect to neutral clusters, due to charge delocalization over several molecules. This phenomenon was previously studied theoretically by Piuzzi and coworkers[50] on aromatic molecules smaller than coronene. Charge delocalization over a few molecules strongly binds these molecules to each other through partially covalent forces. Around the charge core, the remaining (mostly) neutral molecules undergo polarization forces, which are also stronger than standard dispersion and quadrupolar interactions. Thus, the overall cohesion felt by any molecule in a cationic PAH cluster is stronger. Consequently, clustering effects on the vibrational properties should be even larger in the case of singly charged clusters. Unfortunately, the collective effect of charge delocalization cannot be described using simple explicit potentials, and its modeling is an important task in itself.[50] Despite these limitations, we believe that the trends found here should be rather general, and we hope they will be a first step in preparing and interpreting the Herschel observational campaign.

Acknowledgment. M.R. acknowledges financial support from the Von Humboldt fundation. F.C. wishes to thank Tim James for significant help with the OPTIM calculations. The simulations have been carried out on the CALMIP computer center, which we gratefully acknowledge. We also thank the anonymous reviewers for useful suggestions in improving the manuscript.

References and Notes

(1) Bakker, J. M.; Aleese, L. M.; Meijer, G.; von Helden, G. *Phys. Rev. Lett.* **2003**, *91*, 203003.
(2) Kapota, C.; Lemaire, J.; Maître, P.; Ohanessian, G. *J. Am. Chem. Soc.* **2004**, *126*, 1836.
(3) Chin, W; Piuzzi, F.; Dimicoli, I.; Mons, M. *Phys. Chem. Chem. Phys.* **2006**, *8*, 1033.
(4) Lorenz, U.; Solca, N.; Dopfer, O. *Chem. Phys. Lett.* **2005**, *406*, 321.
(5) Ramos, C.; Winter, P. R.; Stearns, J. A.; Zwier, T. S. *J. Phys. Chem. A* **2003**, *107*, 10280.
(6) Zwier, T. S. *Annu. Rev. Phys. Chem.* **1996**, *47*, 205.
(7) Ebata, T.; Fujii, A.; Mikami, N. *Int. Rev. Phys. Chem.* **1998**, *17*, 331.
(8) Buck, U.; Huisken, F. *Chem. Rev.* **2000**, *3863*, 100.
(9) Beu, T. A.; Buck, U. *J. Chem. Phys.* **2001**, *114*, 7848.
(10) Roscioli, J. R.; Hammer, N. I.; Johnson, M. A. *J. Phys. Chem. A* **2006**, *110*, 7517.
(11) Léger, A.; Puger, J. L. *Astron. Astroph.* **1984**, *137*, L5.
(12) Allamandola, L. J.; Tielens, A. G. G. M.; Barker, J. R. *Astrophys. J. Lett.* **1985**, *290*, L25.
(13) Boulanger, F. In *New Perspectives on the Interstellar Medium, ASP Conference Series 168*; Taylor, A. R., Landecker, T. L., Joncas., G., Ed.; Astronomical Society of the Pacific: San Francisco, CA, 1999; p 173.
(14) Szczepanski, J.; Vala, M. *Astrophys. J.* **1993**, *414*, 646.
(15) Hudgins, D.; Allamandola, L. *J. Phys. Chem.* **1995**, *99*, 3003.
(16) Hudgins, D. M.; Allamandola, L. J. *Astrophys. J. Lett.* **1999**, *516*, L41.
(17) Mattioda, A. L.; Hudgins, D. M.; Bauschlicher, C. W. J.; Rose, M.; Allamandola, L. J. *J. Phys. Chem. A* **203**, *107*, 1486.
(18) Huneycutt, A. J.; Casaes, R. N.; Saykally, R. J.; Chung, C.-Y.; Lee, Y.-P. *Chem. Phys. Chem.* **2004**, *5*, 321.
(19) Kurtz, J. *Astron. Astrophys.* **1993**, *255*, L1.
(20) Joblin, C.; Boissel, P.; Léger, A.; D'Hendecourt, L.; Defourneau, D. *Astron. Astrophys.* **1995**, *299*, 835.
(21) Cook, D. J.; Saykally, R. J. *Astrophys. J.* **1998**, *493*, 793.
(22) Oomens, J.; van Roij, A. J. A.; Meijer, G.; von Helden, G. *Astrophys. J.* **2000**, *542*, 404.
(23) Oomens, J.; Sartakov, B. G.; Tielens, A. G. G. M; Meijer, G.; von Helden, G. *Astrophys. J. Lett.* **2001**, *560*, L99.
(24) Kim, H.-S.; Wagner, D. R.; Saykally, R. J. *Phys. Rev. Lett.* **2001**, *86*, 5691.
(25) Papanek, P.; Kamitakahara, W. A.; Zhou, P.; Fischer, J. E. *J. Phys.: Condens. Matter* **2001**, *13*, 8287.
(26) Mitchell, P. C. H.; Ramirez-Cuesta, A. J.; Parkern, S. F.; Tomkinson, J. *J. Mol. Struct.* **2003**, *651*−*653*, 781.
(27) Fleischer, U.; Pulay, P. *J. Raman Spectrosc.* **1998**, *29*, 473.
(28) Mapelli, C.; Castiglioni, C.; Zerbi, G.; Müllen, K. *Phys. Rev. B* **1999**, *60*, 12710.
(29) de Frees, D. J.; Miller, M. D.; Talbi, D.; Pauzat, F.; Ellinger, Y. *Astrophys. J.* **1993**, *408*, 530.
(30) Pauzat, F.; Talbi, D.; Ellinger, Y. *Astron. Astrophys.* **1995**, *293*, 263.
(31) Langhoff, S. *J. Phys. Chem.* **1996**, *100*, 2819.
(32) Martin, J. M. L. *Chem. Phys. Lett.* **1996**, *262*, 97.
(33) Ellinger, Y.; Pauzat, F.; Lengsfield, B. H. *J. Mol. Struct.* **1999**, *458*, 203.
(34) Pauzat, F.; Ellinger, Y. *Chem. Phys.* **2002**, *280*, 267.
(35) Bauschlicher, C. W. J. *Astrophys. J.* **2002**, *564*, 782.
(36) Hudgins, M.; Bauschlicher, C. W. J.; Allamandola, L. J. *Spectrochim. Acta A: Mol. Biomol. Spectrosc.* **2001**, *57*, 907.

(37) Pauzat, F.; Ellinger, Y. *Mon. Not. R. Astron. Soc.* **2001**, *324*, 355.
(38) Sallamie, N.; Shaw, J. M. *Fluid Phase Equilib.* **2005**, *237*, 100.
(39) Malloci, G.; Joblin, C.; Mulas, G. *Chem. Phys.* **2007**, *332*, 353.
(40) Cesarsky, D.; Lequeux, J.; Ryter, C.; Gérin, M. *Astron. Astrophys.* **2000**, *354*, L87.
(41) Rapacioli, M.; Joblin, C.; Boissel, P. *Astron. Astrophys.* **2005**, *429*, 193.
(42) Berné, O.; Joblin, C.; Deville, Y.; Smith, J.; Rapacioli, M.; Bernard, J.; Thomas, J.; Reach, W.; Abergel, A. *Astron. Astrophys.*, in press.
(43) Joblin, C.; Toublanc, D.; Boissel, P.; Tielens, A. G. G. M. *Mol. Phys.* **2002**, *100*, 3595.
(44) Mulas, G.; Malloci, G.; Joblin, C.; Toublanc, D. *Astron. Astrophys.* **2006**, *460*, 93.
(45) Richter, H.; Howard, J. B. *Prog. Energy Combust. Sci.* **2000**, *265*, 26.
(46) Reilly, P. T. A.; Gieray, R. A.; Whitten, W. B.; Ramsey, J. M. *Combust. Flame* **2000**, *122*, 90.
(47) Keller, A.; Kovacs, R.; Homann, K.-H. *Phys. Chem. Chem. Phys.* **2000**, *2*, 1667.
(48) Benharash, P.; Gleason, M. J.; Felker, P. M. *J. Phys. Chem. A* **1999**, *103*, 1442.
(49) Song, J. K.; Lee, N. K.; Kim, J. H.; Han, S. Y.; Kim, S. K. *J. Chem. Phys.* **2003**, *119*, 3071.
(50) Piuzzi, F.; Dimicoli, I.; Mons, M.; Millié, P.; Brenner, V.; Zhao, Q.; Soep, B.; Tramer, A. *Chem. Phys.* **2002**, *275*, 123.
(51) Miller, J. H.; Mallard, W. G.; Smyth, K. C. *J. Phys. Chem.* **1984**, *88*, 4963.
(52) van de Waal, B. *J. Chem. Phys.* **1983**, *79*, 3948.
(53) Chen, E. S.; Chen, E. C. M.; Sane, N.; Talley, L.; Kozanecki, N.; Sculze, S. *J. Chem. Phys.* **1999**, *110*, 9319.
(54) Conzales, C.; Lim, E. *J. Phys. Chem.* **1999**, *103*, 1437.
(55) Marzec, A. *Carbon* **2000**, *38*, 1863.
(56) Ruuska, H.; Pakkanen, T. A. *J. Phys. Chem. B* **2001**, *105*, 9541.
(57) Grimme, S. *J. Comput. Chem.* **2004**, *25*, 1463.
(58) Bréchignac, P.; Schmidt, M.; Masson, A.; Pino, T.; Parneix, P.; Bréchignac, C. *Astron. Astrophys.* **2005**, *442*, 239.
(59) Schmidt, M.; Masson, A.; Bréchignac, C. *Int. J. Mass. Spectrom.* **2006**, *252*, 173.
(60) Rapacioli, M.; Calvo, F.; Spiegelman, F.; Joblin, C.; Wales, D. J. *J. Phys. Chem. A* **2005**, *109*, 2487.
(61) Rapacioli, M.; Calvo, F.; Joblin, C.; Parneix, P.; Toublanc, D.; Spiegelman, F. *Astron. Astrophys.* **2006**, *460*, 519.
(62) Seahra, S. S.; Duley, W. W. *Astrophys. J.* **2000**, *542*, 898.
(63) Van Oanh, N. T.; Parneix, P.; Bréchignac, P. *J. Phys. Chem. A* **2002**, *106*, 10144.
(64) Klots, C. *J. Phys. Chem.* **1971**, *75*, 10.
(65) Léger, A.; Boissel, P.; Désert, F. X.; D'Hendecourt, L. *Astron. Astroph.* **1989**, *213*, 351.
(66) Wong, W.-K.; Westrum, E. F.; Jr. *J. Chem. Thermodyn.* **1971**, *3*, 105.
(67) Chickos, J. S.; Acree, W. A., Jr.; Liebman, J. F. *J. Phys. Chem. Ref. Data* **1999**, *28*, 1535.
(68) Chickos, J. S.; Webb, P.; Nichols, G.; Kiyobayashi, T.; Cheng, P.-C.; Scott, L. *J. Chem. Thermodyn.* **2002**, *34*, 1195.
(69) Pitzer, K. S.; Gwinn, W. D. *J. Chem. Phys.* **1942**, *10*, 428.
(70) Cyvin, S. J.; Cyvin, B. N.; Brunvoll, J.; Whitmer, J. C.; Klaeboe, P. *Z. Naturforsch., Teil A* **1982**, *37*, 1359.
(71) Murry, R. L.; Fourkas, J. T.; Li, W.-X.; Keyes, T. *J. Chem. Phys.* **1999**, *110*, 10410.
(72) Wales, D. J. *OPTIM version 3.2: A program for optimizing geometries and calculating reaction pathways*; URL http://www-wales.ch.cam.ac.uk/OPTIM/.
(73) Wales, D. J. *Philos. Trans. R. Soc. London, A* **2005**, *363*, 357.
(74) Pirali, O.; Nguyen-Thi, V.-O.; Vervloet, M.; Parneix, P.; Bréchignac, Ph. *Phys. Chem. Chem. Phys.* **2006**, *8*, 3707.
(75) The data in our previous paper[60] were erroneously labelled as μm, instead of cm^{-1}.
(76) Calvo, F. *J. Chem. Phys.* **2005**, *123*, 124106.
(77) Isaacson, A. D.; Truhlar, D. G. *J. Chem. Phys.* **1981**, *75*, 4090.
(78) Labastie, P.; Whetten, R. L. *Phys. Rev. Lett.* **1990**, *65*, 1567.
(79) Berry, R. S.; Smirnov, B. M. *J. Chem. Phys.* **2001**, *114*, 6816.
(80) Hill, T. L. *Thermodynamics of small systems*; Dover: New York, 1963.
(81) Imry, Y. *Phys. Rev. B* **1980**, *21*, 2042.
(82) Calvo, F. *J. Phys. Chem. B* **2001**, *105*, 2183.
(83) Ferreira, A. L. C.; Pacheco, J. M.; Prates-Ramalho, J. P. *J. Chem. Phys.* **2000**, *113*, 738.
(84) Seifert, G.; Porezag, D.; Frauenheim, T. *Int. J. Quantum Chem.* **1996**, *58*, 185.
(85) Elstner, M.; Porezag, D.; Jungnickel, G.; Elsner, J.; Haugk, M.; Frauenheil, T.; Suhai, S.; Seifert, G. *Phys. Rev. B* **1998**, *58*, 7260.
(86) Martinez, M.; Gaigeot, M.-P.; Borgis, D.; Vuilleumier, R. *J. Chem. Phys.* **2006**, *125*, 144106.
(87) Allamandola, L. J.; Tielens, A. G. G. M.; Barker, J. R. *Astrophys. J. Suppl.* **1989**, *71*, 733.